MASTER COPY KEEP THIS COPY FOR REPRODUCTION PURPOSES

TATION PAGE

Form Approved
OMB No 0704-0188

AD-A234 775

2. DATE	3. REPORT TYPE AND DATES COVERED
February 23, 1991	

4. TITLE AND SUBTITLE
DYNAMICS OF ELASTIC BENDING AND TORSION OF HINGELESS ROTORS WITH DYNAMIC STALL

5. FUNDING NUMBERS
DAAL03-87-K-0037

6. AUTHOR(S)
Gopal H. Gaonkar and Dinesh Barwey

7. PERFORMING ORGANIZATION NAME(S) AND ADDRESS(ES)
Department of Mechanical Engineering
Florida Atlantic University
Boca Raton, Florida 33431

8. PERFORMING ORGANIZATION REPORT NUMBER

APR 1 1991

9. SPONSORING/MONITORING AGENCY NAME(S) AND ADDRESS(ES)
U. S. Army Research Office
P. O. Box 12211
Research Triangle Park, NC 27709-2211

10. SPONSORING/MONITORING AGENCY REPORT NUMBER
ARO 24738.7-EG

11. SUPPLEMENTARY NOTES
The view, opinions and/or findings contained in this report are those of the author(s) and should not be construed as an official Department of the Army position, policy, or decision, unless so designated by other documentation.

12a. DISTRIBUTION/AVAILABILITY STATEMENT
Approved for public release; distribution unlimited.

12b. DISTRIBUTION CODE

13. ABSTRACT *(Maximum 200 words)*
The effects of dynamic stall lift and drag on the flap-lag stability of a hingeless rotor are investigated, both experimentally and analytically. The emphasis is on the correlation with measured regressing lead-lag mode damping levels of a soft-inplane, three-bladed model rotor, operated untrimmed. The correlation covers awide range of test conditions for several values of rotor speed, collective pitch angle, shaft tilt angle and advanve ratio. It includes cases that vary from near zero thrust conditions in hover to highly stalled forward flight conditions with advance ratios as high as 0.55 and shaft tilt angles as high as 20°. Both the experimental and analytical blade models represent a simple model of a hingeless rotor with rigid blades and spring restrained flap-lag hinges. The aerodynamic representation is based on the ONERA dynamic stall models comprising virtually independent unified lift and drag models. The nonlinear equations of blade motion and stall dynamics are perturbed about a periodic forced response, and the damping is evaluated by the Floquet eigenanalysis. In comparison to the linear and quasisteady stall aerodynamic theories, the theory with dynamic stall lift and quasisteady stall drag qualitatively improves the correlation, and adding dynamic stall drag provides further quantitative improvement.

14. SUBJECT TERMS
Dynamic Stall Lift and Drag, Lag Damping, Correlation, Hingeless Rotor

15. NUMBER OF PAGES
50

16. PRICE CODE

17. SECURITY CLASSIFICATION OF REPORT	18. SECURITY CLASSIFICATION OF THIS PAGE	19. SECURITY CLASSIFICATION OF ABSTRACT	20. LIMITATION OF ABSTRACT
UNCLASSIFIED	UNCLASSIFIED	UNCLASSIFIED	UL

TABLE OF CONTENTS

	Table of Contents	i
	Summary	ii
	Notations	iii
	List of Tables and Figures	vi
1	Introduction	1
2	Experiment and Data	3
3	Analytical Model	4
	3 1 Dynamic Stall Modeling	5
	3 2 Blade Equations	9
	3 3 Solution Scheme	10
4	Results	11
	4 1 Forced Response	12
	4 2 Lag Damping Correlation	13
5	Conclusions	19
	Bibliography	21
	List of Publications	43
	List of Personnel Supported	43

Summary

The effects of dynamic stall lift and drag on the flap-lag stability of a hingeless rotor are investigated, both experimentally and analytically. The emphasis is on the correlation with measured regressing lead-lag mode damping levels of a soft-inplane, three-bladed model rotor, operated untrimmed. The correlation covers a wide range of test conditions for several values of rotor speed, collective pitch angle, shaft tilt angle and advance ratio. It includes cases that vary from near zero thrust condition in hover to highly stalled forward-flight conditions with advance ratios as high as 0.55 and shaft tilt angles as high as 20°. Both the experimental and analytical blade models represent a simple model of a hingeless rotor with rigid blades and spring restrained flap-lag hinges. The aerodynamic representation is based on the ONERA dynamic stall models comprising virtually independent unified lift and drag models. The nonlinear equations of blade motion and stall dynamics are perturbed about a periodic forced response, and the damping is evaluated by the Floquet eigenanalysis. In comparison to the linear and quasisteady stall aerodynamic theories, the theory with dynamic stall lift and quasisteady stall drag qualitatively improves the correlation, and adding dynamic stall drag provides further quantitative improvement.

Notation

Unless otherwise stated, the symbols below are nondimensional

a	linear lift curve slope, rad^{-1}
a_d	damping factor for dynamic stall drag
b	blade semi-chord, (1/R)
c	blade chord, m
C_d, C_l	airfoil sectional drag and lift coefficients
C_{ds}	quasisteady stall drag coefficient
C_{d_o}	airfoil constant profile drag coefficient
C_{l_o}	airfoil lift coefficient at zero angle of attack
C_T	thrust coefficient
C_{zl}, C_{zs}	linear and quasisteady stall lift coefficient
C_β	nonrotating flap damping coefficient
C_ζ	nonrotating lead–lag damping coefficient
D	airfoil drag force per unit length in the free-stream direction, $(1/\rho\, b\, \Omega^2 R^2)$
e_h	blade hinge offset, (1/R)
e	phase shift parameter for dynamic stall lift
e_d	phase shift parameter for dynamic stall drag
F_β, F_ζ	airloads per unit length in flap and lead-lag directions
k	b/r
k_r	reduced frequency, Fig 4
L	airfoil lift force per unit length normal to the free-stream, $(1/\rho\, b\, \Omega^2 R^2)$
L_o	apparent mass lift normal to the chord line, $(1/\rho\, b\, \Omega^2 R^2)$
N	number of blade segments
P	flap stiffness parameter
r	radial distance from rotor center, (1/R)
r_d	dynamic stall drag frequency parameter

R	rotor radius, *in*
s	apparent mass parameter, πd^{-1}
U	resultant air velocity at a blade section, $(1/\Omega R)$
U_P, U_T	local air velocities components in the rotor hub plane, $(1/\Omega R)$
w	dynamic stall lift frequency parameter
W	lead-lag stiffness parameter
z	blade radial distance measured from the hinge, (1/R)
x, y	local blade-fixed coordinates
Z	flap-lag stiffness parameter
α	blade airfoil section angle of attack, *rad*
α_c	camber of the airfoil, *rad*
α_{ss}	quasisteady stall angle, *rad*
α_s	shaft tilt angle, *rad*
β	blade flapping angle, *rad*
γ	lock number
Γ	circulation per unit length, UC_l
Γ_d	Circulation-like drag per unit length, UC_d
Δ_i	width of the ith aerodynamic element
δ	pitch-rate coefficient, rad^{-1}
$\dot{\epsilon}$	airfoil rotation rate with respect to the airmass
ζ	blade lead-lag angle, *rad*
λ	time delay parameter
λ_i	total inflow ratio
θ	blade pitch angle, *rad*
θ_0	collective pitch angle, *rad*, *deg*
μ	advance ratio
σ	negative of lead-lag mode damping exponent, sec^{-1}

σ_s	rotor solidity
ϕ	blade section inflow angle, Fig. 2
ψ	nondimensional time or blade azimuthal position, *rad*
ω_e	frequency term due to blade hinge offset
ω_ζ	rotating lead-lag frequency, $(1/\Omega)$
$\omega_{\beta_0}, \omega_{\zeta_0}$	nonrotating flap and lead-lag frequencies, $(1/\Omega)$
Ω	rotor angular speed, *rad/sec*
$(\,)_i$	ith blade segment
$(\,)_1, (\,)_2$	unstalled and stalled components
$(\,)_x, (\,)_y$	x and y components
$(\,)'$	$d(\,)/d\psi$
$(\bar{\ })$	equilibrium state
$(\,)$	perturbed state

List of Tables and Figures

Table 1	Experimental Model Rotor I Properties	23
Table 2	Baseline Parameters	24
Fig 1	Rotor Model Test Conditions in Hover and forward flight	25
Fig 2	Sectional Aerodynamic Forces and Velocities	26
Fig 3	Quasisteady and Linear Lift Coefficients versus Angle of Attack	27
Fig 4	Effect of Stall Parameter δ on Lift Hysteresis Loops of NACA 23012 Airfoil	28
Fig 5	Quasisteady and Linear Drag Profiles for Low Reynolds Number Flow	29
Fig 6	Periodic Flap Response in Forward Flight, $\mu = 0.35$, $\alpha_s = 20°$	30
Fig 7	Equilibrium Local Angles of Attack Variations, $\mu = 0.35$, $\alpha_s = 20°$	31
Fig 8	Thrust Levels in Forward Flight for Varying Shaft Tilt	32
Fig 9	Lag Mode Damping Correlation in Hover	33
Fig 10	Effect of Stall Lift Parameter δ on Lag Damping Predictions in Forward Flight	34

Fig 11 : Lag Damping Correlation in Forward Flight for Low Shaft Angles, $\theta_c = 0°$ 35

Fig. 12 : Lag Damping Correlation in Forward Flight for Low Shaft Angles, $\theta_0 = 3°$ 36

Fig. 13 : Lag Damping Correlation in Forward Flight for High Shaft Angles, $\theta_0 = 0°$ 37

Fig. 14 : Lag Damping Correlation in Forward Flight for High Shaft Angles, $\theta_0 = 3°$ 39

Fig. 15 : Lag Damping Correlation in Forward Flight, $\theta_0 = 6°$ 40

Fig. 16 : Summary of Lag Damping Correlation in Forward Flight 41

Fig. 17 : Adequacy of Linear Theory in Forward Flight 42

1. Introduction

Very little is known about rotor blade stability under dynamically stalled conditions in forward flight. This is particularly true of lead-lag or lag modes that are at best weakly damped and for which current methods of predicting damping levels merit considerable refinement. Given the complexity of the flow field of a rotor blade in dynamic stall, it is important that analytical results are compared with a broad range of experimental data. Accordingly, the present study investigates the effects of dynamic stall lift and dynamic stall drag on the flap-lag stability of an isolated hingeless rotor. The emphasis is on the correlation of analytical lead-lag damping results with experimental data from tests performed on a three-bladed isolated model rotor in the U.S. Army Aeroflightdynamics Directorate's 7- by 10-foot (2.1 m by 3.0 m) wind tunnel (Ref.1). The experimental model represents a simple model of a hingeless rotor with rigid blades having spring restrained flap and lag hinges. This intentional simplicity helps to focus the testing on the main topics of interest, which are the forward flight and dynamic stall aspects of the stability problem. The structural details of the analytical model were chosen to correspond as closely as possible to the experimental model to remove possible sources of error in the correlation. The database comprises lag regressing mode damping and covers a wide range of test conditions for various values of rotor speed (Ω), collective pitch (θ_0), shaft angle (α_s), and advance ratio (μ). It includes cases that vary from near zero thrust conditions in hover to highly stalled forward flight conditions with advance ratios up to 0.55 and shaft tilt angles to 20°.

The present work originated as part of a research program to validate new analytical methods based on Floquet theory for predicting the effects of forward flight on aeroelastic stability of rotorcraft. The work of Ref. 2 on flap-lag dynamics of an isolated blade is a typical early application of Floquet theory to solve the periodic coefficient equations that arise in forward flight. Virtually no systematic correlations exist that

address the validity of such Floquet theory, even though it is now in relatively widespread use. The Aeroflightdynamics Directorate undertook a carefully designed small-scale model testing program to obtain data for such validations. The results of the experimental tests are reported in Ref. 1, where the effects of periodic excitations in forward flight presented no particular pr[illegible]em in extracting lag damping from transient response data Comparisons with theory are reported in Refs. 3 4. In Ref. 3, the prediction is based on linear quasisteady aerodynamic theory with a dynamic inflow unsteady wake theory The results were satisfactory only for very low values of collective pitch and advance ratio and it was suspected that the effects of airfoil stall might be responsible. In an attempt to explain the reasons for the poor correlation, the emphasis of the investigation shifted to the examination of the influence of airfoil stall on forward flight aeroelastic stability Earlier studies (e g. Ref 5), comparing quasisteady aerodynamic theory with experimental data for the hover flight condition had shown that airfoil stall strongly influenced flap-lag stability in hover at high collective pitch angles and, furthermore, that quasisteady nonlinear airfoil stall characteristics could successfully account for these influences. Consequently, these effects were included in the forward flight flap-lag studies in Ref 4. For hover and very low advance ratios, the anticipated improvements were largely realized, however, the results for high advance ratios were poor and, paradoxically, in some cases even worse than the linear theory correlation. As a result, the present investigation was undertaken and a nonlinear dynamic stall theory was included in the analytical predictions

Rotor blades in forward flight encounter a highly complex three-dimensional unsteady flow field, which typically includes regions that for many operating conditions are partly stalled. Several dynamic stall models have been developed and used to predict time histories as well as damping levels (Refs. 6-10). In this paper, the aerodynamic description is based on the ONERA dynamic stall unified lift and drag models (Refs. 6 and 7) The nonlinear equations of blade and stall dynamics are perturbed about a periodic forced response to compute damping levels from the Floquet eigenanalysis The emphasis is on

demonstrating the need for including dynamic stall in the prediction of lag damping, not on the relative merits of different dynamic stall models or of the Floquet stability analysis vis-a-vis other stability analysis methods. Given the breadth of the study, this correlation will provide a reference comparison with other correlation studies based on different approaches to modeling dynamic stall and to predicting stability margins. It will also help clarify the effects of dynamic stall on the lag stability of isolated rotors.

2. Experiment and Data

A brief account of the experimental model and database is given here (for details see Ref. 1). To enable the use of a simple rigid flap-lag analysis for correlation, the three-bladed rotor used flexures to simulate hinged blades with spring restraint and coincident flap and lag hinges, the effective hinge offset was 0.11R. The untapered rotor blades had no pretwist and were stiff relative to the flap and lag flexures so that the first flap and lag modes essentially involve only rigid-body blade motions. Further, the design ensures a rotating torsional frequency of at least 9/rev over the entire rotor speed range tested and, thus, virtually eliminates the need to consider a torsional degree of freedom. While this model is not representative of an operational rotor system, it is suitable due to the desire to restrict the scope of the physical phenomena being studied for initial research investigations. Future experiments should introduce the blade torsion degree of freedom. The experimental damping data used in the present correlation were obtained from two rotor models of identical design, Rotor I and Rotor II. For example, at the collective pitch angle of zero degree, the damping data were obtained from Rotors I and II, whereas, at the collective pitch of three and six degrees, the data were acquired from tests on Rotor II. Procedures were essentially the same for both the rotors. Owing to manufacturing differences, the lag and torsion stiffnesses, nonrotating flap and lag frequencies and structural flap damping of the rotors differ slightly, but these differences are too small to

be significant. Thus, for the analysis, only the Rotor I properties were used (Table 1), since, the bulk of high advance ratio ($\mu > 0.3$) and high thrust ($C_T/\sigma_s > 0.1$) data refers to model Rotor I(dotted lines in Fig. 1).

The model tested was a 63.84-in diameter three-bladed rotor mounted on a very stiff rotor stand so that the stability data were representative of an isolated rotor The rotor had no cyclic pitch control, and collective pitch was set manually prior to each run At a given advance ratio, rotor speed and collective pitch, the shaft tilt was the only means of controlling the rotor. Thus, the rotor was operated untrimmed with a virtually unrestricted tilt of the tip-path plane. The lack of cyclic blade pitch control prevents trimming the rotor to arbitrarily chosen thrust, propulsive force, flapping, or hub moment conditions, but it does remove a potentially serious source of friction damping from the system and ensures high quality data (Ref. 1). The model was shaken in roll to excite the lag modes and then locked up to record the transient response. The frequency and damping data were then obtained from the time histories via a moving block technique. In forward flight two rotor speeds were used (Ω = 750 and 1000 rpm), corresponding to ω_ζ values of 0 72 and 0 6i Advance ratio, shaft tilt and collective pitch were varied to cover the test envelope shown in Fig 1. At each condition tested, at least two separate damping measurements were obtained.

3. Analytical Model

The mathematical model represents the structural simplicity of the experimental model rotor, as an offset-hinged, rigid blade executing lag(inplane) and flap motions with coincident spring restrained flap and lag hinges. The hinge offset of 11 1% is accounted for, in both the rotor steady state and stability analyses. The rotor is untrimmed, with no cyclic pitch (cyclic flapping present). At a given advance ratio, the collective pitch and shaft tilt angles are the known control input parameters. The principal elastic axes of the

hinges do not rotate with blade collective pitch angle.

3.1 Dynamic Stall Modeling

The aerodynamic representation is based on the ONERA dynamic stall models of unsteady lift and drag, which are virtually independent (Refs 6,7). With Γ representing the instantaneous circulation providing lift, and, Γ_d representing the analogous circulation-like drag counterpart, the stall dynamics begin with the following representation .

$$\Gamma = \Gamma_1 + \Gamma_2 \quad \text{and} \quad \Gamma_d = \Gamma_{d_1} + \Gamma_{d_2} \tag{1}$$

where subscripts 1 and 2 indicate the linear and the nonlinear (stalled) components, respectively. For the local coordinates of Fig. 2, the corresponding dynamic stall lift components are modeled according to Eqs (2) :

$$L_y = U_x(\Gamma_1+\Gamma_2) + U_y(\Gamma_{d_1}+\Gamma_{d_2}) + L_o \tag{2a}$$

$$L_x = -U_y(\Gamma_1+\Gamma_2) + U_x(\Gamma_{d_1}+\Gamma_{d_2}) \tag{2b}$$

$$L_o = b\,s\,\dot{U}_y \tag{2c}$$

$$k\dot{\Gamma}_1 + \lambda\Gamma_1 = \lambda(aU_y\cos\alpha + UC_{l_o}) + \delta\, b\,\dot{\epsilon} \tag{2d}$$

$$\begin{aligned} k^2\ddot{\Gamma}_2 + 2dwk\dot{\Gamma}_2 + w^2(1+d^2)\Gamma_2 = -w^2(1+d^2)\{ & U\Delta C_z \\ & + e\,k(\dot{U}_x\cos\alpha + \dot{U}_y\sin\alpha)\,\Delta C_z \\ & + e\,k\frac{\partial\Delta C_z}{\partial\alpha}(\dot{U}_y\cos\alpha - \dot{U}_x\sin\alpha)\} \end{aligned} \tag{2e}$$

where Γ_1 and Γ_2 represent circulation per unit length for the linear and stalled contributions Moreover, the parameters b, a and s denote the airfoil semi-chord, linear lift curve slope, and apparent mass term, respectively In Eq. (2d), the term UC_{l_o} accounts for

nonzero lift at zero angle of attack and the difference in maximum lift at positive and negative angles of attack of the NACA 23012 airfoil section. The term $\dot{\epsilon}$ signifies the airfoil rotation rate with respect to air mass. Therefore, $\dot{\epsilon}$ must include all geometric rotations of the airfoil, even if they come from sources other than blade pitch. For the rigid flap-lag motion of a rotor blade, $\dot{\epsilon} = \dot{\theta} + (1 + \dot{\zeta}) \sin\beta$. In the absence of cyclic pitch $\dot{\theta}$ is zero; hence, $\dot{\epsilon} = (1 + \dot{\zeta}) \sin\beta$. Further, in Eqs. (2d) and (2e), k reflects an average of the reduced frequency of the free-stream, and coefficients λ, δ, w, d, and e are the stall system parameters. As shown in Fig. 3, ΔC_z is the difference between the extrapolated linear lift coefficient and quasisteady stall lift coefficient in the stalled region. The quasisteady stall lift coefficient, C_{zs}, is approximated by the following functions for angles of attack between 0° and 180°

$$C_{zs} = C_{zl} \qquad 0° \leq \alpha \leq \alpha_{ss}° \qquad (2f)$$

$$C_{zs} = a \sin\alpha_{ss} \cos\alpha_{ss} + C_{l_0} \qquad \alpha_{ss}{}^c < \alpha < 45° \qquad (2g)$$

$$C_{zs} = a \sin\alpha_{ss} \cos\alpha_{ss} \sin 2\alpha + C_{l_0} \qquad 45° \leq \alpha \leq 135° \qquad (2h)$$

$$C_{zs} = -a \sin\alpha_{ss} \cos\alpha_{ss} + C_{l_0} \qquad 135° < \alpha < (180-\alpha_{ss})° \qquad (2i)$$

$$C_{zs} = C_{zl} \qquad (180-\alpha_{ss})° \leq \alpha \leq 180° \qquad (2j)$$

In Eqs. (2e) to (2i), α_{ss} is the quasisteady stall angle, and C_{zl} the extrapolated linear lift coefficient, which, following the unified lift theory, is

$$C_{zl} = a \sin\alpha \cos\alpha + C_{l_0} \qquad 0° \leq \alpha \leq 180° \qquad (2k)$$

To ascertain the lift coefficient values at negative angles of attack, a phase shift of 180° can be applied to α. It is noted that the simplified quasisteady stall model incorporates different maximum lift values at positive and negative stall conditions as expected for the cambered NACA 23012 airfoil section, however, it does not include different positive and negative stall angles of attack.

As seen from Eqs. (2c) to (2e), there are six coefficients of the dynamic stall lift model, identified from wind-tunnel measurements, and for the OA212 airfoil they are well discussed in Ref. 6 It is instructive that δ is the only parameter in the dynamics equation of the unstalled circulation. Eq. (2d), that is dependent on ΔC_z. In a general sense applicable to a series of airfoils including NACA 23012, δ can be approximated as

$$\delta = \partial C_{zl}/\partial\alpha - 0.5c\,(\,1 + 1.43\,|\Delta C_z|\,) \qquad (2l)$$

In the above equation $0.5a$ term gives the same instantaneous step response (normalized lift), one-half the final value, as the Wagner (pitch) function. As emphasized in Ref. 6, despite the differences in airfoils, such responses of normalized lift do exhibit qualitative similarity. A further approximation of δ that appreciably simplifies both the trim and perturbation analyses is to remove dependency on ΔC_z, since δ is expected to primarily influence the unstalled or linear circulation Γ_l, as typified by Eq. (2d). That is,

$$\delta = \partial C_{zl}/\partial\alpha - (a/2) \qquad (2m)$$

Fig. 4 shows the effect of this approximation on the dynamic stall lift coefficient for the NACA 23012 airfoil, the experimental data is from Ref. 11 at 1×10^6 Reynolds number. Thus, Eq. (2m) provides a viable approximation that is consistent with the classical linear unsteady lift theory. Also, it removes the ΔC_z -dependency of the unstalled circulation Γ_l. In Fig. 4, the effects of further simplification in δ, which neglects the second term in Eq. (2m), are also shown. It is seen that this approximation is also a reasonable alternative for obtaining a qualitative trend However. it instantaneously gives the normalized lift response that is equal to the final value of the Wagner function and, thus, violates the time delay in the classical linear unsteady theory (Ref. 6). Hereafter, δ according to Eq. (2m) is used in the dynamic stall lift theory unless noted otherwise (see Fig. 10, which explores sensitivity of lag damping to such change in δ).

As seen from Fig. 2, the resultant velocity U and the angle of attack α are given by

$$U = \sqrt{U_P^2 + U_T^2} = \sqrt{U_x^2 + U_y^2} \quad : \quad \alpha = \arctan(U_y/U_x) \tag{3a}$$

where

$$U_T = e_h \cos\zeta + \cos\beta\,(1+\dot{\zeta})\,x + \mu \sin(\psi+\zeta) \tag{3b}$$

$$U_P = -e_h \sin\zeta \sin\beta + x\dot{\beta} + \lambda_t \cos^2 + \mu \sin\beta \cos(\psi+\zeta) \tag{3c}$$

$$U_x = U_T \cos\theta_o + U_P \sin\theta_o \tag{3d}$$

$$U_y = U_T \sin\theta_o - U_P \cos\theta_o \tag{3e}$$

The dynamic stall drag model follows the same analytical structure of the lift model, except that the linear component Γ_{d_1} in Eq. (1) does not involve an additional state. The dynamic stall drag suitable for use in conjunction with the dynamic stall lift model is formulated according to the following equations:

$$\Gamma_{d_1} = U\,C_{d_o} \tag{4a}$$

$$k^2 \ddot{\Gamma}_{d_2} + a_d k \dot{\Gamma}_{d_2} + r_d^2 \Gamma_{d_2} = -\left[\, r_d^2\, U\, \Delta C_d + e_d k \dot{U}_y \,\right] \tag{4b}$$

where ΔC_d, as shown in Fig. 5a, indicates the difference between the constant profile drag coefficient and the quasisteady stall drag coefficient, analogous to ΔC_z in Fig 3. The above formulation of dynamic drag in terms of circulation-like drag variables attempts to incorporate the unsteady wind-speed variations and the heaving motion of the airfoil, analogous to the circulation lift model.

For substall conditions with positive angles of attack (e g hover data in Fig. 1), Refs. 1 and 12 suggest the following expression for the quasisteady stall drag.

$$C_{d_s} = 0\,0079 + 1\,7\,\alpha^2 \tag{4c}$$

According to Ref. 1, Eq (4c) is based on steady-bending-moment data from a test with the blades similar to those used in the present test. However, the present test also includes

stalled cases in forward flight, both with positive and negative angles of attack The quasisteady stall drag data appropriate to the database of Fig. 1 are not available, and the present study uses the following equation :

$$C_{ds} = 1.03 - (1.03 - C_{d_o}) \cos 2(\alpha + \alpha_c), \qquad -180^\circ \leq \alpha \leq 180^\circ \tag{4d}$$

As seen from Fig. 5,there are quantitative differences between Eqs. (4d) and (4c) for moderate angles of attack. But over the large angle of attack of range Eq (4d) agrees well with Eq. (4c), behaves smoothly for a complete sweep of angle of attack, and is, thus, expected to be adequate in predicting qualitatively the principal effects of quasisteady stall drag on lag damping.

For the ONERA OA212 airfoil, the dynamic stall lift parameters are well discussed in Ref. 6. By comparison, the dynamic stall drag model is still evolving, and its parameters in Eq. (4b) are assumed to be:

$$a_d = 0.32\,, \quad r_d = 0.2 + 0.1\,\Delta C_z^2\,, \text{ and } \quad e_d = -0.015\,\Delta C_z^2 \tag{5}$$

3.2 Blade Equations

To implement the dynamic stall lift and drag effects according to Eqs (2) and (4), the blade is discretized into N radial aerodynamic elements, and the aerodynamic forces are assumed to be constant in each element. Accordingly, the rigid flap-lag equations take the form :

$$\ddot{\beta} + C_\beta \dot{\beta} + \sin\beta\cos\beta(1+\dot{\zeta})^2 + \omega_\zeta^2 \sin\beta\cos\zeta + (P-1)\beta + Z\zeta = \frac{\gamma}{2a} \sum_{i=1}^{N} F_{\beta_i} r_i \Delta_i \tag{6a}$$

$$\cos^2\beta\,\ddot{\zeta} + C_{\zeta}\,\dot{\zeta} - 2\sin\beta\cos\beta(1+\dot{\zeta})\dot{\beta} + \omega_{\zeta}^2\cos\beta\sin\zeta + W\zeta + Z\beta$$

$$= \frac{\gamma}{2a}\cos\beta\sum_{i=1}^{N} F_{\zeta_i}\, r_i\, \Delta_i \qquad (6b)$$

In Eqs. (6), F_{β_i} and F_{ζ_i} are the dimensionless airloads, acting at the center of the ith element, perpendicular to the blade and, respectively, perpendicular and parallel to the plane of rotation. Moreover, r_i represents the radial location of the center of the ith element from the blade hinge, and Δ_i is the length of the ith element. The stiffness parameters P, W and Z in Eqs. (6) are defined in Ref. 2. For this study, $P = 1+\omega_{\beta_o}^2$, $W = \omega_{\zeta_o}^2$, and $Z = 0$.

According to Eqs. (2), (3) and (4), the flap and lag aerodynamic forces for a generic ith blade element can be expressed as

$$F_{\beta_i} = \left[(\Gamma_1+\Gamma_2)\, U_T - U_P\,(\Gamma_{d_1}+\Gamma_{d_2}) + L_o\cos\theta_o \right]_i \qquad (7a)$$

$$F_{\zeta_i} = -\left[(\Gamma_1+\Gamma_2)\, U_P + U_T\,(\Gamma_{d_1}+\Gamma_{d_2}) + L_o\sin\theta_o \right]_i \qquad (7b)$$

3.3 Solution Scheme

Concerning trim and Floquet eigenanalysis, a few details are added here for completeness. The rotor is operated with specified control inputs for collective pitch angle θ_o and shaft tilt α_s. Since cyclic pitch inputs were not used, the rotor is not trimmed to a specified force or moment condition. The equilibrium conditions are found by time integration over several rotor revolutions until convergence or response periodicity is achieved. Determination of uniform steady inflow and thrust is based on the momentum theory. It must be emphasized that the test conditions deviate significantly from typical helicopter rotor operations (e.g. large negative thrust and coning, shaft tilt as high as 20° and advance ratio varying from zero to 0.55). The stability margins or damping levels are

computed from a standard eigenanalysis of the Floquet transition matrix (FTM), which was generated by a single-pass initial value code. Computational reliability is verified on the basis of eigenvalue condition numbers and residual errors of eigenpairs (Ref. 13)

A consistent perturbation scheme requires that all quantities depending on angle of attack be perturbed about a periodic forced response with equilibrium angle of attack $\bar{\alpha}$ For example, with $\underline{\alpha} = \alpha - \bar{\alpha}$, the corresponding perturbations in the circulation of the ith element, ΔC_z and ΔC_d, are

$$\underline{\Gamma}_{1i} = \Gamma_{1i} - \bar{\Gamma}_{1i} \tag{8a}$$

$$\underline{\Gamma}_{2i} = \Gamma_{2i} - \bar{\Gamma}_{2i} \tag{8b}$$

$$\Delta C_z = (\Delta C_z)_{\bar{\alpha}} + \left[\frac{\partial \Delta C_z}{\partial \alpha}\right]_{\bar{\alpha}} \underline{\alpha} \tag{8c}$$

$$\frac{\partial \Delta C_z}{\partial \alpha} = \left[\frac{\partial \Delta C_z}{\partial \alpha}\right]_{\bar{\alpha}} + \left[\frac{\partial^2 \Delta C_z}{\partial \alpha^2}\right]_{\bar{\alpha}} \underline{\alpha} \tag{8d}$$

$$\Delta C_d = (\Delta C_d)_{\bar{\alpha}} + \left[\frac{\partial \Delta C_d}{\partial \alpha}\right]_{\bar{\alpha}} \underline{\alpha} \tag{8e}$$

Though the required perturbation per se is fairly routine, Eqs. (8a) and (8b) are mentioned to emphasize the role of individual discretized elements, and Eqs (8c), (8d) and (8e) are mentioned to emphasize the role of quasisteady stall lift and drag characteristics It also should be emphasized that the dynamic stall lift parameters δ, w, d and e in Eqs (2), and dynamic stall drag parameters r_d and e_d in Eq. (5) depend upon the angle of attack and require perturbation.

4. Results

If not stated otherwise the results in Figs. 6 to 17 are based on the baseline values given in Table 2, and specific additional values are so identified in respective figures The lag damping predictions are based on the uniform steady inflow The following four theories

are examined. 1) *linear theory*, a constant airfoil lift-curve slope and profile drag coefficient with no reverse flow (Figs. 6–16) and with reverse flow (Fig 17), 2) *quasisteady stall theory*, linear theory refined to include quasisteady nonlinear airfoil lift and drag characteristics which include reverse flow effects (Figs. 3 and 5), 3) *dynamic stall lift theory*, quasisteady stall theory refined to include dynamic stall lift, and 4) *dynamic stall theory*, which includes dynamic stall lift and dynamic stall drag characteristics of the airfoil. Given the extensive scope of the database represented in Fig. 1, only a portion of the correlation is presented.

4.1 Forced Response

Figs. 6 and 7 show, respectively, the trim results of periodic flap-response β and angle of attack $\bar{\alpha}$ over one rotor revolution. All three collective pitch angles of the database in forward flight (also see Fig. 1) are considered for an advance ratio of 0.35 and shaft tilt angle of 20°. While Fig. 6 shows the flapping response from the linear, quasisteady stall and dynamic stall theories, Fig. 7 shows the angle of attack results from only the dynamic stall theory for the three outer blade elements. For brevity, $\bar{\alpha}$ predictions from the linear and quasisteady stall theories for the entire blade are omitted. Similarly, $\bar{\alpha}$ predictions from the dynamic stall theory for the two inner segments are omitted as well, although the inner segments experience much higher angles of attack, they are aerodynamically less effective. As seen from Fig. 6, both dynamic stall and quasisteady stall effects increase with decreasing collective pitch for this high shaft tilt case with $\alpha_s = 20°$. Also, as stall effects increase the linear theory β results deviate significantly from those of the stall theories. The $\bar{\alpha}$ predictions in Fig. 7 support the β predictions in Fig. 6, in which the maximum magnitude of the local angle of attack $\bar{\alpha}$ decreases substantially as collective pitch increases. Another feature merits special attention . most of the blade experiences negative angles of attack $\bar{\alpha}$ with particularly large magnitudes for the zero collective-pitch case. This is a result of the test conditions chosen for the experimental model, which at zero collective

pitch angle and at high advance ratios experienced large negative angles of attack and coning angles (Ref. 1). Since the blade airfoil is cambered, these negative angles of attack stall conditions represent an unusual operating condition for the airfoil For the higher collective pitch angles of 3° and 6°, the stall regions shrink noticeably on the retreating blade, particularly near the blade-tip where $\bar{\alpha}$ essentially remains unstalled, e g see Figs 7b and 7c for the outermost fourth and fifth elements.

The dynamic stall effects on the trim results are further pursued in Fig. 8, in which thrust levels C_T/σ_s based on the linear theory are shown. Results for dynamic stall theory (not shown) indicated that the linear theory overpredicted C_T/σ_s by about 25% for $\theta_o = 0°$ at $\mu = 0\ 35$. Nevertheless, Fig. 8 serves as a rough guideline in illustrating the interdependence of thrust and stalled conditions For example, comparison of Figs 6 and 8 shows that the quasisteady stall and dynamic stall effects are more pronounced at the high thrust conditions. Regarding the database in Fig. 1, the trim results in Figs 6, 7 and 8 show that dynamic stall should play a major role for the 0° collective case. particularly for the high-advance-ratio and high-shaft-tilt combinations. That role should be minor for $\theta_o = 3°$ and 6°, the higher the collective pitch, the less the dynamic stall effects

4.2 Lag Damping Correlation

The following damping predictions are based on the nonlinear quasisteady drag characteristics using Eq. (4d). Fig. 9 shows lag damping versus rotational speed in hover for collective pitch angles $\theta_o = 4°$ and 8°. Here, the dynamic stall effects are negligible, as determined from the stall angles based on the trim values ($|$angle of attack $\bar{\alpha}| \leq 12°$) The predictions cluster into two groups of linear theory vis-a-vis the other three theories. The linear theory is fairly adequate in the prediction of damping level trends, including the reduction in damping level around 375 rpm, where the flap and lag frequencies coalesce. However, the discrepancies between the data and the linear theory consistently increase for $\Omega > 450$ rpm. By comparison, the remaining three theories provide excellent correlation

throughout. The difference between the three stall theories and the linear theory is primarily due to the nonlinear drag effects. Furthermore, the difference between the quasisteady stall theory and the dynamic stall theories is rather small overall, but consistently increases with increasing collective pitch and rotational speed, it illustrates the the linear unsteady lift effects, since, stall is not an issue here.

The lag damping correlation in forward flight is treated in Figs. 10 to 17 for a complete range of advance ratio ($0 \leq \mu \leq 0.55$) and collective pitch angle ($\theta_o = 0°$, 3° and 6°), with the shaft tilt angle α_s varying from 0° to 20°. Fig. 10 shows the effects of simplifying δ according to Eq. (2m) on lag mode damping, and, thus, it complements the results in Fig. 4. The damping is presented versus advance ratio, the shaft angle $\alpha_s = 16°$ for both collective pitch angles of 0° and 3°, and $\alpha_s = 20°$ for collective pitch angle of 6° The predictions are based on the dynamic stall lift theory for two representations of δ according to Eq. (2l), and simplification according to Eq. (2m). With increasing advance ratio, both predictions show the same trend of an initial reduction in the damping followed by an abrupt increase in the damping. That this trend is not sensitive to such changes in δ is an appealing feature of the dynamic stall lift model.

Fig. 11 shows lag damping versus advance ratio for shaft tilt $\alpha_s = 0°$ and 4°, both at 0° collective pitch angle. For these shaft tilt angles, the thrust levels $|C_T/\sigma_s|$ are very low for all advance ratios with a maximum value of about 0.03 (see Fig 8a) This is well reflected by the almost identical predictions from all four theories for $\mu < 0.4$ At advance ratios above 0.4, the linear theory predicts higher values than the stall theories, and this deviation from the stall theories and the data increases with increasing advance ratio On the other hand, the quasisteady stall and dynamic stall lift theories continue to predict almost identical values for $\mu > 0.4$. Thus shows negligible effects of dynamic stall lift, including unsteady lift in substall for $\theta_o = 0°$. Further study shows that the deviation of the linear theory for $\mu > 0.40$ is associated with very high lift prediction due to the assumption of constant lift curve slope and no reverse flow.

As seen from Fig. 12, the lag damping correlation is continued for 3° collective pitch angle for three relatively low values of shaft tilt, $\alpha_s = 0°$, 4° and 8°. Here also the thrust level $|C_T/\sigma_s|$ is relatively low and it generally decreases with increasing shaft tilt (see Fig 8b). The data are available for the low advance ratio range, $\mu < 0.3$, and all four theories correlate well with data. Thus, for $\mu < 0.3$, the quasisteady stall, dynamic stall lift and dynamic stall theories predict essentially the same damping, and the linear theory deviates from these three theories mainly due to nonlinear drag effects in substall. Thus, at low shaft tilt angles treated in Figs 11 and 12, the quasisteady stall theory and the two dynamic stall theories provide excellent correlation.

The damping correlation at relatively high shaft tilt angles, $\alpha_s = 8°$, 12°, 16° and 20°, at $\theta_0 = 0°$, is given in Fig. 13. Up to advance ratio of about 0.2 ($|C_T/\sigma_s| < 0.06$), the predicted damping essentially remains constant, all four theories are virtually identical and correlate well with the data. For advance ratio $\mu > 0.25$, the data show that the damping increases rather abruptly, this abruptness being more marked with increasing shaft tilt α_s and advance ratio μ. Fig. 8a facilitates a better understanding of this abrupt and marked increase in damping. It shows that the thrust level varies from –0.07 at $\alpha_s = 8°$ to –0.23 at $\alpha_s = 20°$, basically representing high negative thrust and highly stalled conditions. Surprisingly, the linear theory predicts this trend of abruptly and markedly increasing damping. The quasisteady stall theory eventually predicts this peculiarity, however, the structure or pattern of this increase is different from that of the data, especially at shaft tilt angles of 16° and 20° for which quasisteady stall theory predicts mild instability and then shows the abrupt increase. But inclusion of dynamic stall lift effects brings in significant quantitative improvement in the correlation, more or less qualitative improvement at high shaft tilts of 16° and 20°. Inclusion of dynamic stall drag yields further quantitative improvement. It must be mentioned that these improvements of dynamic stall lift and dynamic stall drag are consistent in that the improvements increase markedly with increasing advance ratio It must be noted however, that overall, the linear

theory gives the best correlation for the case of zero collective pitch angle.

The correlation for 3° collective pitch angle is given in Fig. 14 for high shaft tilt angles, $\alpha_s \geq 12°$. The data show the clear trend of slowly decreasing damping with increasing advance ratio However, the linear theory is qualitatively inaccurate here, predicting the opposite trend of rather rapidly increasing damping with increasing advance ratio. The other three theories cluster together and predict the trend of the data better. A significant observation is that the three stall theories for high μ and α_s combinations (say $\mu > 0.4$ and $\alpha_s \geq 14$) predict an abruptly increasing damping, as do the linear theory in general and the data in Fig. 13 for $\theta_0 = 0°$ in particular. In the absence of experimental data at high μ for $\theta_0 = 3°$, it is difficult to judge the validity of the dynamic stall theory here.

The correlation for the 6° collective pitch angle is shown in Fig. 15 for $\alpha_s = 20°$ and is quite similar to that in Fig. 14 where the damping slowly decreases with increasing advance ratio. This trend is well predicted by the quasisteady stall, dynamic stall lift and dynamic stall theories. In contrast, the linear theory is qualitatively inaccurate. The improvement over the linear theory by the quasisteady stall theory is significant and reflects the nonlinear drag effects on lag damping. The dynamic stall theories deviate marginally from the quasisteady stall theory mainly due to the unsteady linear lift effects. With increasing advance ratio, particularly for $\mu > 0.4$, the dynamic stall lift and dynamic stall drag come into play. As in the previous case for $\theta_0 = 3°$ in Fig 14, here also it is not possible to validate such high-advance-ratio predictions on the basis of test data.

To facilitate an overall assessment of the adequacy of the four theories for a wide range of data in forward flight, Fig. 16 shows a summary of the correlation for the collective pitch angles of 0°, 3° and 6° at high shaft tilt angles of 14°, 14° and 20°, respectively. The predictions of linear and quasisteady stall theories are unsatisfactory, each providing good correlation for one or two cases and qualitatively inaccurate prediction for the remaining cases. For example, the linear theory gives good correlation for the case

of zero collective pitch angle, Fig 15a. But for 3° and 6° collective pitch angles, Figs. 16b and 16c, it predicts increasing damping with increasing advance ratio which is qualitatively inaccurate in comparison with the test data In contrast, quasisteady stall theory gives good correlation for collective pitch angles $\theta_0 = 3°$ and 6°. However, for $\theta_0 = 0°$, quasisteady stall theory is both quantitatively and qualitatively inaccurate. On the other hand, the dynamic stall lift theory provides the crucial correction for $\theta_0 = 0°$ and gives fairly accurate prediction in all three cases. In other words, quasisteady stall theory refined to include dynamic stall consistently provides the best correlation for the broadest range of experimental data. Furthermore, it should be noted that the linear theory in highly separated flow conditions, for the collective pitch angle of zero degree at high shaft tilts, provides surprisingly adequate correlation.

The summary results in Fig. 16 may also be interpreted in terms of the variation of thrust level with advance ratio. In Fig. 16a, C_T/σ_s varies from roughly 0 to –0.1 over the advance ratio range of 0 to 0.4. In Fig. 16b, C_T/σ_s varies from 0.025 to –0.045, and in Fig. 16c from 0.05 to –0.05 Therefore, Fig 16a changes from low thrust to high negative thrust with significant airfoil stall. Fig. 16b changes from moderate positive thrust to moderate negative thrust with moderate stall, and Fig. 16c changes from high positive to moderate negative thrust with similarly moderate airfoil stall.

With respect to the effect of rotor thrust level and advance ratio on theoretical predictions of lead-lag damping, the following observations can be made. For both linear and nonlinear theories, the basic trend is for damping to increase with advance ratio after an intermediate reduction in damping from the nonlinear theories. This basic trend can be interpreted as the result of two effects known to influence the lead-lag damping. 1) the effect of thrust variation with advance ratio and 2) periodic coefficient effects due to advance ratio The basic difference between the linear and nonlinear theory is that the nonlinear theory predicts that the damping decreases before the increased trend takes place. This initial decrease in the damping is related to the reduced lift prediction by the

stall theories. Comparing the nonlinear stall theories, it is interesting that the effect of dynamic stall in forward flight tends to offset the large influence of quasistatic stall on lead-lag damping, although this compensation is small for hover and low advance ratios.

From Fig. 16a (also Figs. 13), it is seen that the earlier-used conventional linear theory, $C_l \propto a\,\alpha$, provides a very satisfactory correlation at $\theta_o = 0^o$. This adequacy of the linear theory for the highly stalled conditions is surprising and merits reassessment. As noted earlier, this linear theory assumes a constant lift-curve slope which predicts unrealistically high lift at large incidence and, also excludes reverse flow effects, an exclusion that further augments over-prediction of lift. The linear theory was refined according to Eq. (2k), $C_l \propto a \sin\alpha \cos\alpha$, to account for the large angles of attack and reverse flow effects, henceforth referred to as the refined linear theory. Accounting for reverse flow according to Eq. (2k) may not be the most accurate way, but, it does incorporate the correct sign reversal in the lift and also predicts a more realistic lift (see Fig. 3). Fig. 17 compares the the refined linear theory with the linear theory, which assumes a constant lift-curve slope and no reverse flow. While the solid lines in Figs. 17 correspond to the refined linear theory, the broken lines correspond to the linear theory without reverse flow effects, as used in Figs 9 to 16. The three cases are identical to those in Fig. 16. It is seen from Fig 17 that the refined linear theory qualitatively alters the damping predictions. For example, at zero collective pitch, Fig 17a shows that the refined linear theory fails to capture the increasing damping-level trend of the test data for high advance ratios. In fact, it shows decreasing damping in contrast to the predictions from the linear theory without reverse flow. Fig. 17b also shows the significant effects of large incidences, but, significantly enough, the refined linear theory predictions are closer to the test data. For the case of $\theta_o = 6^o$ at shaft tilt of 20^o, Fig. 17c shows that both the versions of the linear theory fail to capture the trend of the test data adequately. Overall, Fig. 17 demonstrates that even the refined linear theory is not viable at high advance ratios when the blade encounters high angles of incidence. Moreover, the seeming adequacy of the linear

theory without reverse flow for the isolated case of zero degree collective pitch is erroneous.

The relative prediction capabilities of the various theories may be summarized. The linear theory is successful when the rotor thrust level is low, i.e., when both the collective pitch and advance ratio are low (as in Fig. 16a) or when a combination of high collective pitch offsets a high shaft angle (as in Fig. 16c at an advance ratio near 0.25). The quasisteady stall theory is adequate when thrust level is moderately high and advance ratio is low (as in hover, Fig. 9, and Fig. 16c at low advance ratio). It is interesting to note that a continuous shift between these two conditions is exhibited in Fig. 16c where quasisteady stall successfully predicts the increased damping compared to linear theory for high thrust in hover, but the two predictions begin to merge near an advance ratio of 0.15 when airfoil stall effects vanish as the thrust level drops to zero. Finally, the dynamic stall theory is the most effective theory when both the thrust level and the advance ratio are large.

5. Conclusions

The detailed analytical investigations and correlation of lag damping with the experimental data lead to the following major findings :

1) Conventional Floquet analysis with ONERA unified dynamic stall lift and drag models provide a viable approach for predicting lag-mode damping in stalled forward flight conditions.

2) For low-advance-ratio cases ($\mu \leq 0.20$), the nonlinear substall lift and mainly drag characteristics of the airfoil section significantly improve the correlation with the low-Reynolds-number model test data, confirming earlier analytical and experimental investigations restricted to hovering conditions.

3) The linear theory with constant lift-curve slope is not reliable except when the rotor thrust is low. Its seeming adequacy for the collective pitch of zero degree is erroneous, due to neglecting the effects of large angles of attack and reverse flow. Overall, the refined

linear theory. accounting for the large angles of attack and reverse flow effects, qualitatively differs from the linear theory without refinements, but it is also found to be inadequate except when the rotor thrust is low.

4) The quasisteady stall theory is a significant improvement over the linear theories, without and with refinements, when the advance ratio is low. However it overpredicts the effect of stall at higher advance ratios.

5) Overall, the dynamic stall lift theory provides significant and consistent quantitative and qualitative improvement over the quasisteady stall theory and is found to be viable for the entire database

6) Dynamic stall drag generally provides further quantitative improvement.

7) The lack of sufficient experimental data for high thrust, and moderate-to-high advance ratio conditions limits the ability to fully evaluate the complex character of the prediction methods. Furthermore, the low Reynolds number, and the negatively stalled conditions of the cambered airfoil should be removed in future experimental investigations.

Bibliography

1. McNulty, M.J., "Flap-Lag Stability Data for a Small Scale Isolated Hingeless Rotor in Forward Flight," NASA TM 102189, April 1989.

2. Peters, D.A., " Flap-Lag Stability of Helicopter Rotor Blades in Forward Flight," *Journal of the American Helicopter Society*, Vol. 20, (4), October 1975.

3. Gaonkar, G.H., McNulty, M.J. and Nagabhushanam, J.N., "An Experimental and Analytical Investigation of Isolated Rotor Flap-Lag Stability in Forward Flight," *Journal of The American Helicopter Society*, Vol. 35, (2), April 1990.

4. Nagabhushanam, J.N., Gaonkar, G.H. and McNulty, M.J., "An Experimental and Analytical Investigation of Stall Effects on Flap-Lag Stability in Forward Flight," Thirteenth European Rotorcraft Forum, Arles, France, September 1987.

5. Ormiston, R.A. and Bousman, W.G., "A Study of Stall Induced Flap-Lag Instability of Hingeless Rotors," *Journal of the American Helicopter Society*, Vol. 20, (1), January 1975.

6. Peters, D.A., "Toward a Unified Lift Model for Use in Rotor Blade Stability Analysis," *Journal of The American Helicopter Society*, Vol. 30, (3), July 1985.

7. Petot, D. and Dat, R., "Unsteady Aerodynamic Forces on an Airfoil Performing Oscillations with Unsteady Stall," The Second Technical Workshop on Dynamics and Aeroelastic Stability Modeling of Rotorcraft Systems, Army Research Office and Florida Atlantic University, Boca Raton, Florida, November 1987.

8 Leishman, J.G. and Beddoes, T.S., "A Semi-Empirical Model for Dynamic Stall," *Journal of The American Helicopter Society*, Vol. 34, (3), July 1989.

9. Leishman, J.G. and Crouse, G.L., "State-Space Model for Unsteady Airfoil Behavior and Dynamic Stall," AIAA/ASME/ASCE/AHS/ASC Thirtieth Structures, Structural Dynamics and Materials Conference, Mobile, Alabama, April 1989.

10. Tasker, F.A. and Chopra, I., "Nonlinear Damping Estimation from Rotor Stability Data Using Time and Frequency Domain Techniques," *Journal of The American Helicopter*

Society, Vol. 35, (1), January 1990.

11. Leishman, J.G., Seto, L.Y. and Galbraith, R.A.McD., " Collected Data for Sinusoidal Tests on a NACA 23012 Aerofoil", G.U. Aero Report 8600, University of Glasgow, 1986.

12. Bousman, W.G., Sharpe, D.L. and Ormiston, R.A., "An Experimental Study of Techniques for Increasing the Lead-Lag Damping of Soft Inplane Hingeless Rotors," American Helicopter Society 32nd Annual National V/STOL Forum, Washington D.C., May 1976.

13. Ravichandran, S. et al. "A Study of Symbolic Processing and Computational Aspects in Helicopter Dynamics," *Journal of Sound and Vibration*, Vol. 137, (3), March 1990.

Table 1 : Experimental Model Rotor I Properties

Number of blades	3
Airfoil section	NACA 23012
Hover blade-tip Mach number at 1000 rpm	0.25
Hover blade-tip Reynolds number at 1000 rpm	240,000
Rotor radius, *in*	31.92
Blade chord, *in*	1.65
Radial location of the center of flexures, *in*	3.55
Radial location of the blade center of mass, *in*	11.10
Mass outboard of the flexure center, *slugs*	0.013
Flap/lag inertia about flexure center, *slugs-in*^{2}	1.8
Torsional inertia, *slugs-in*^{2}	0.00294
Flexure assembly flap stiffness, *in-lb/rad*	66.0
Flexure assembly lag stiffness, *in-lb/rad*	281.0
Flexure assembly torsional stiffness, *in-lb/rad*	215.0
Nonrotating flap frequency, *Hz*	3.09
Nonrotating lag frequency, *Hz*	6.98
Nonrotating torsion frequency, *Hz*	149
Nonrotating flap damping, *sec*$^{-1}$	– 0.15
Nonrotating lag damping, *sec*$^{-1}$	– 0 09
Blade pretwist	0.0

Table 2 : Baseline Parameters*

Lift curve slope, a, rad^{-1}	5.73
Lock number, γ (based on a=5.73)	7.54
Profile drag coefficient, C_{d_o}	0.0079
Camber of NACA 23012 airfoil, α_c	1.5°
Lift coefficient at α=0°, C_{l_o}	0.15
Quasisteady stall angle of NACA 23012 airfoil, α_{ss}	±12°
Rotor solidity, σ_s	0.0494
Nondimensional hinge offset, e_h	0.111
Nondimensional blade root cutout	0.186
Rotor speed, Ω	1000 rpm
Number of blade segments, N	5
Apparent mass quantity, s	0.0

*Other structural parameters corresponding to the experimental rotor are given in Table 1.

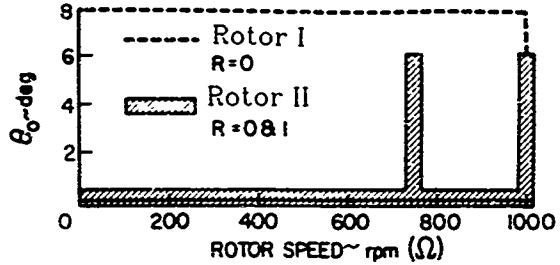

HOVER TESTS (μ=0)

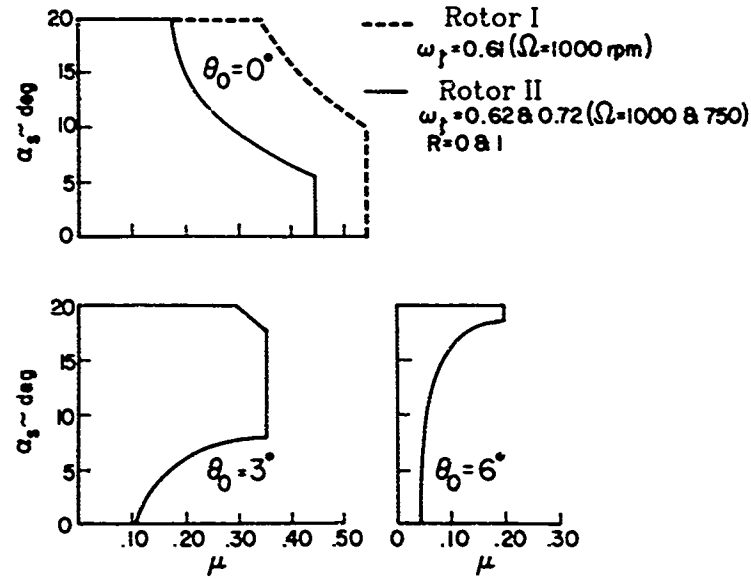

FORWARD FLIGHT TESTS

FIG. 1 ROTOR MODEL TEST CONDITIONS IN HOVER AND FORWARD FLIGHT.

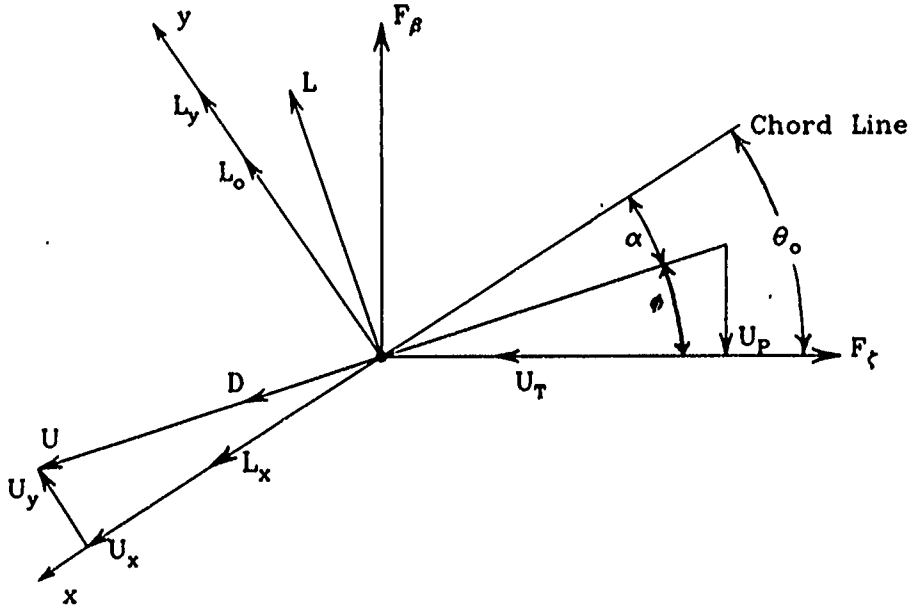

Figure 2 : Sectional aerodynamic forces and velocities

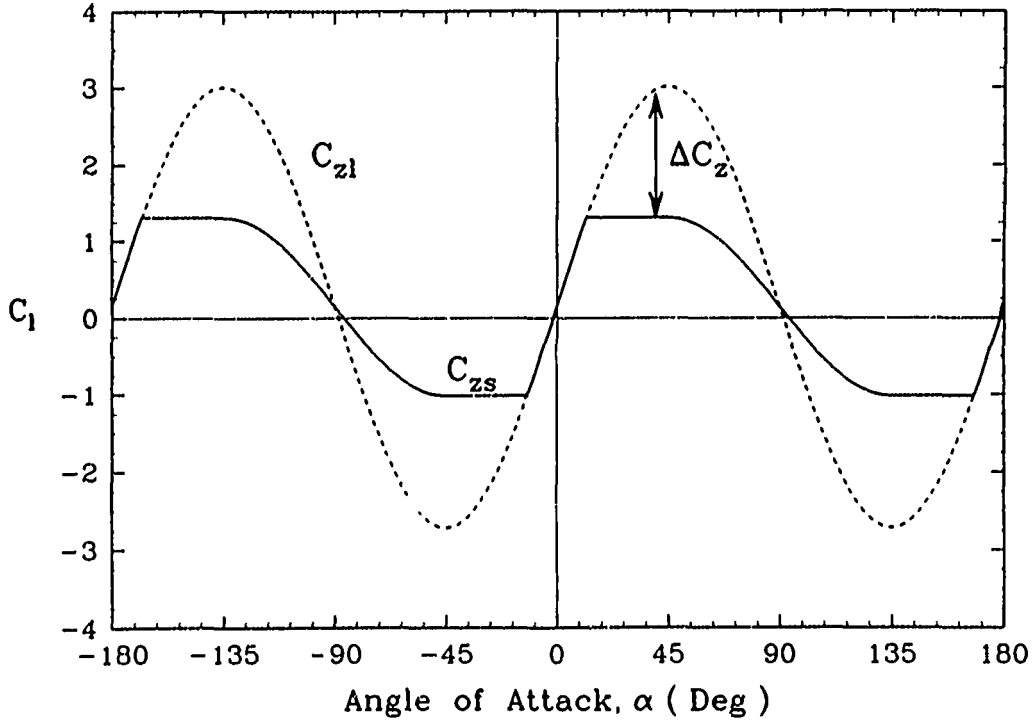

Fig. 3 : Quasisteady and Linear Lift Coefficient versus Angle of AAtack

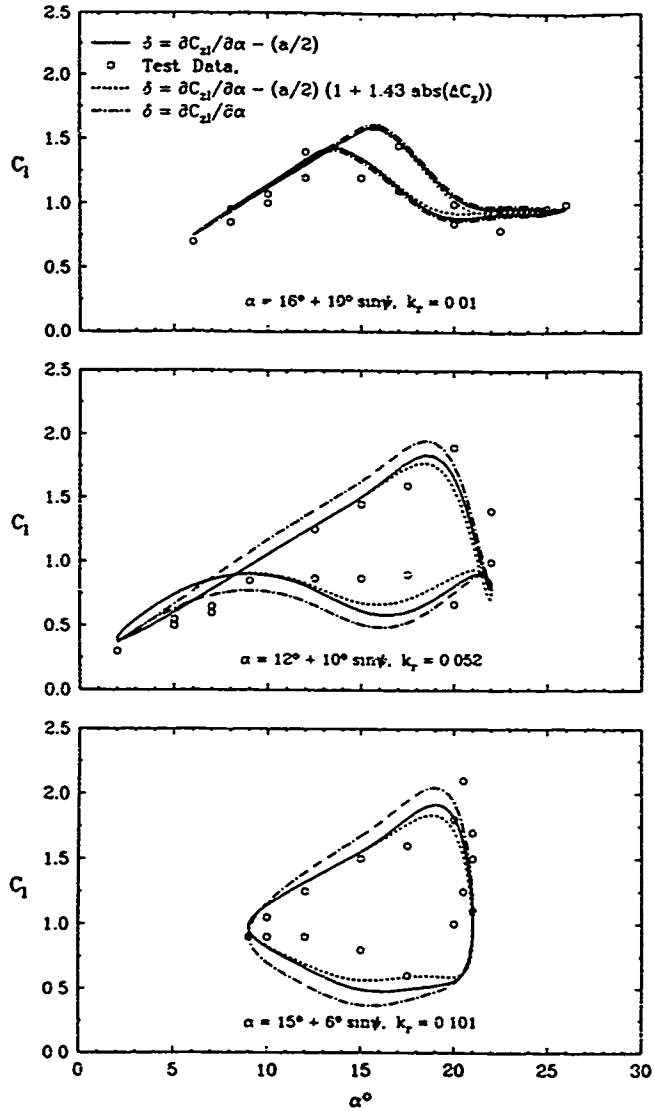

Fig. 4 : Effect of Stall Parameter δ on Lift Hysteresis Loops of NACA 23012 Airfoil

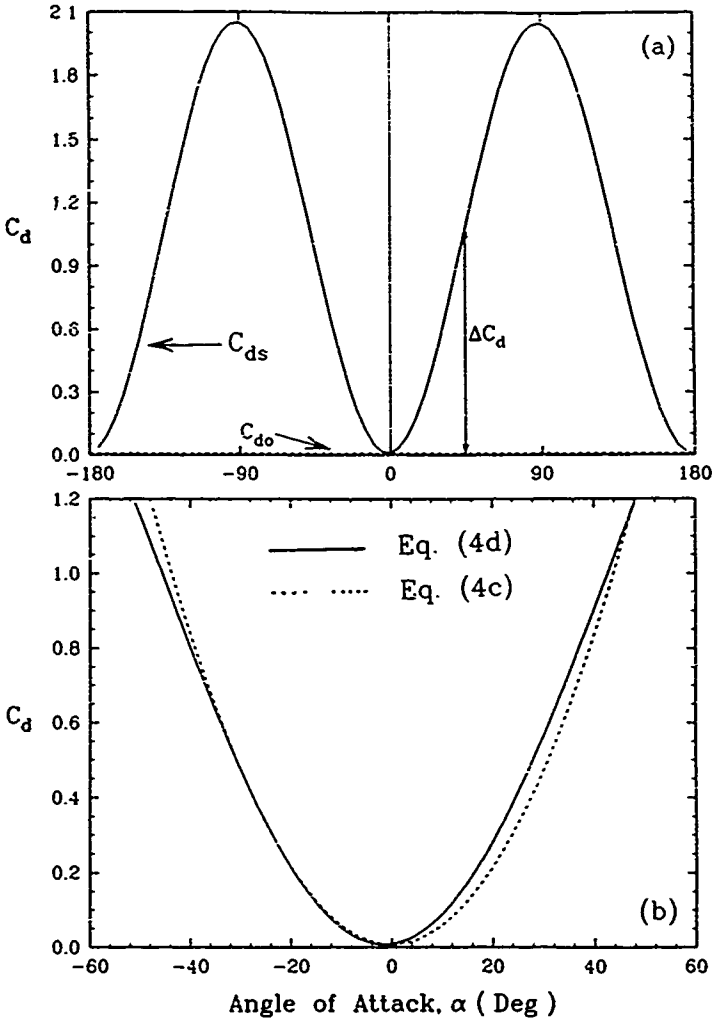

Fig. 5 : Quasisteady and Linear Drag Profiles for Low Reynolds Number Flow

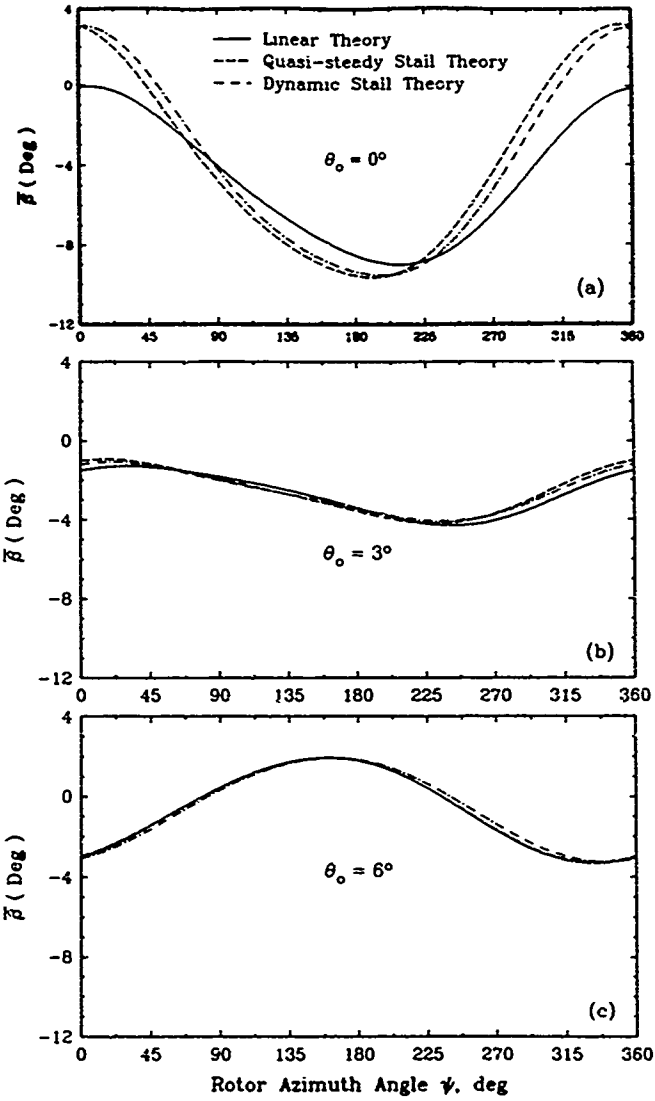

Fig. 5 Periodic Flap Response in Forward Flight, $\mu = 0.35$, $\alpha_s = 20°$

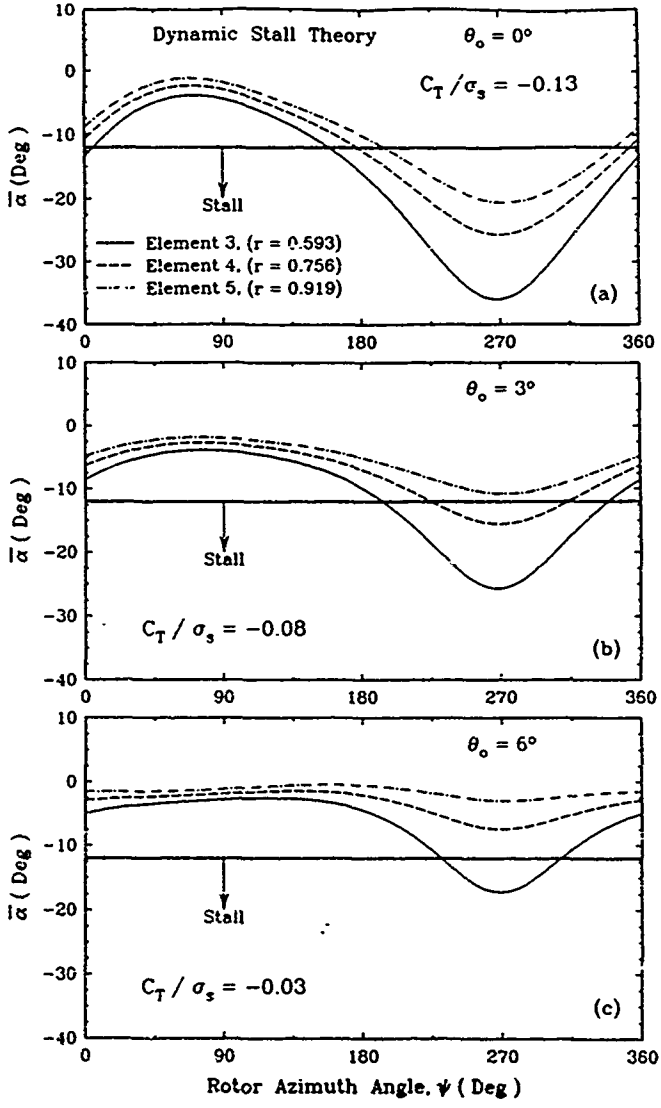

Fig. 7 Equilibrium Local Angles of Attack Variations, $\mu = 0.35$, $\alpha_s = 20°$

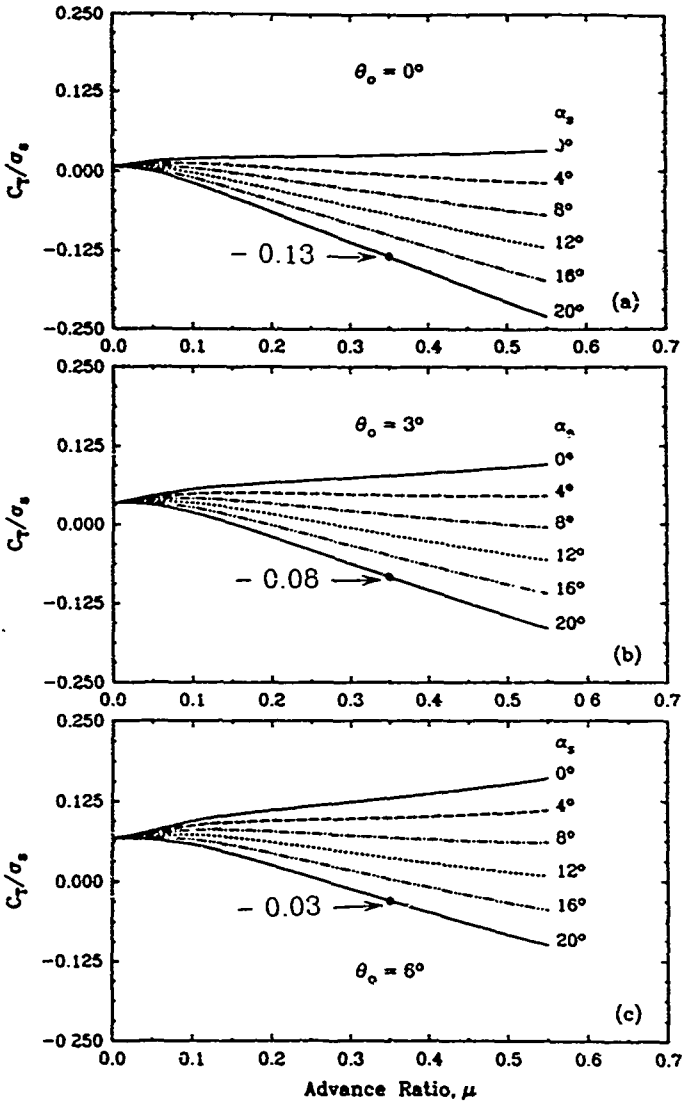

Fig. 8 . Thrust Levels in Forward Flight for Varying Shaft Tilt

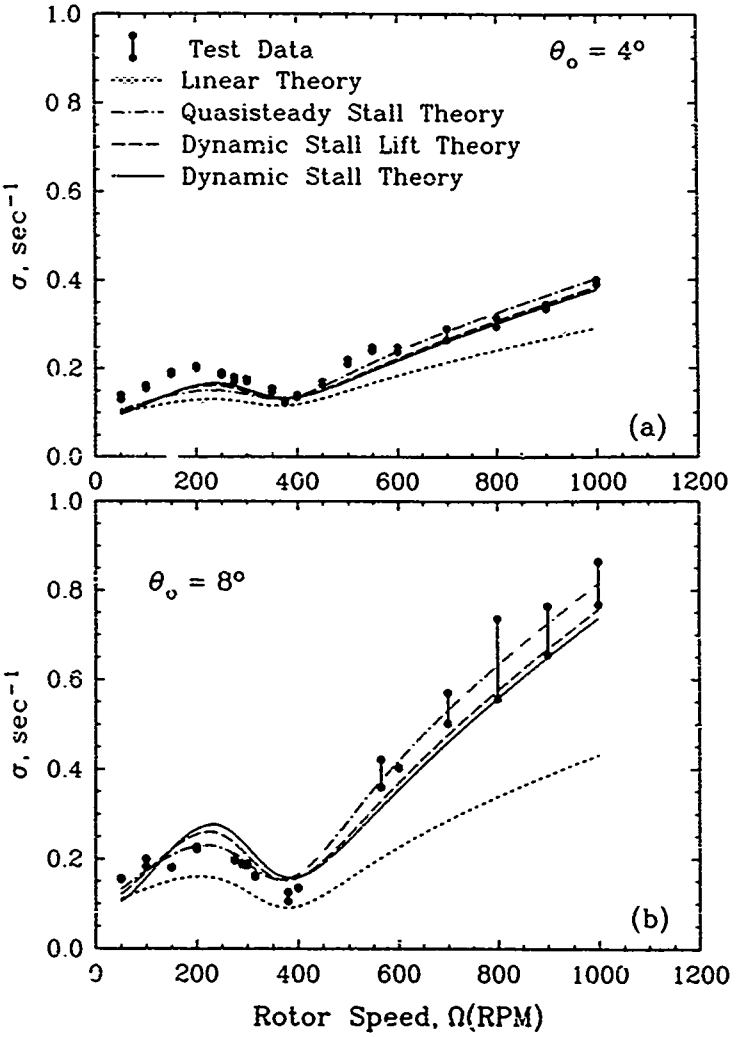

Fig 9 : Lag Mode Damping Correlation in Hover

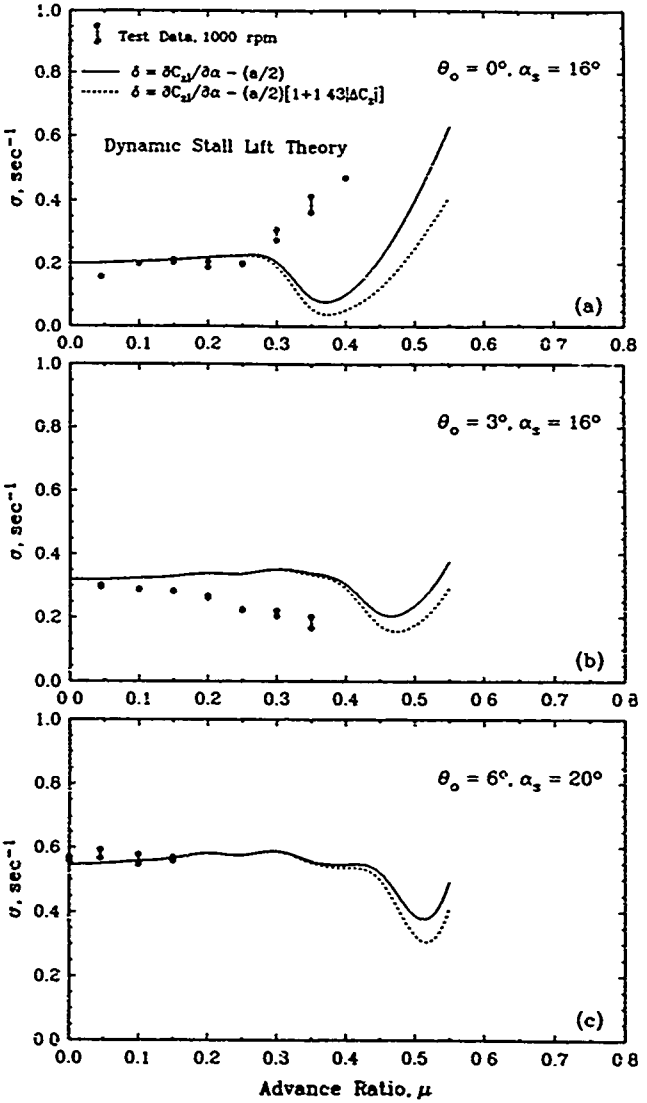

Fig 10 Effect of Stall Lift Parameter δ on Lag Damping Predictions in Forward Flight

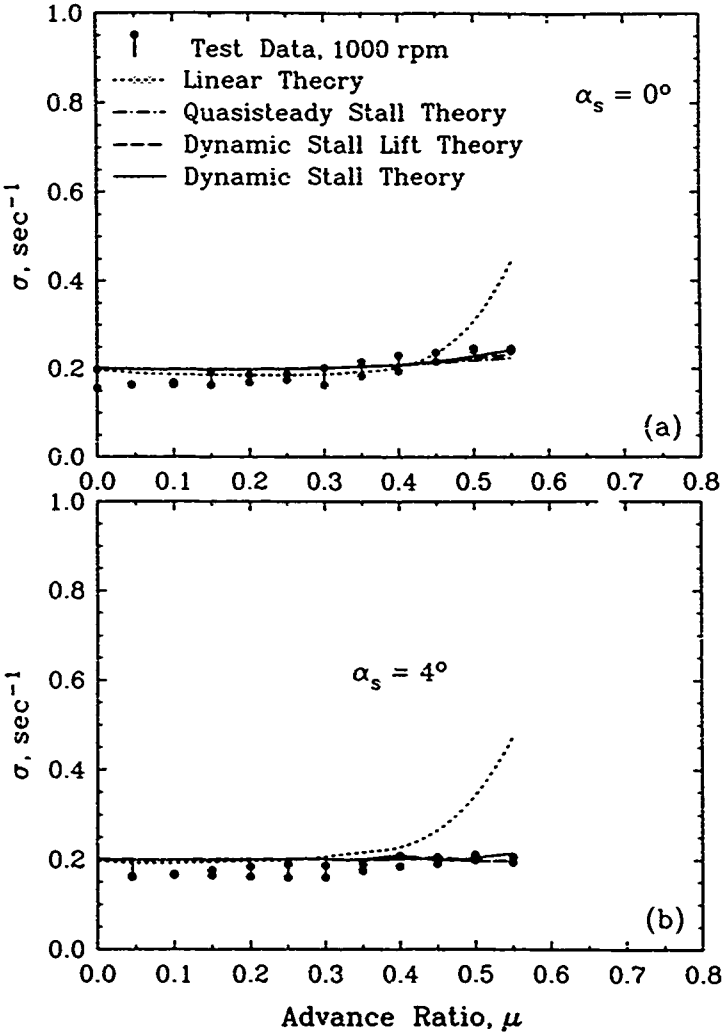

Fig. 11 : Lag Damping Correlation in Forward Flight for Low Shaft Angles, $\theta_o = 0°$

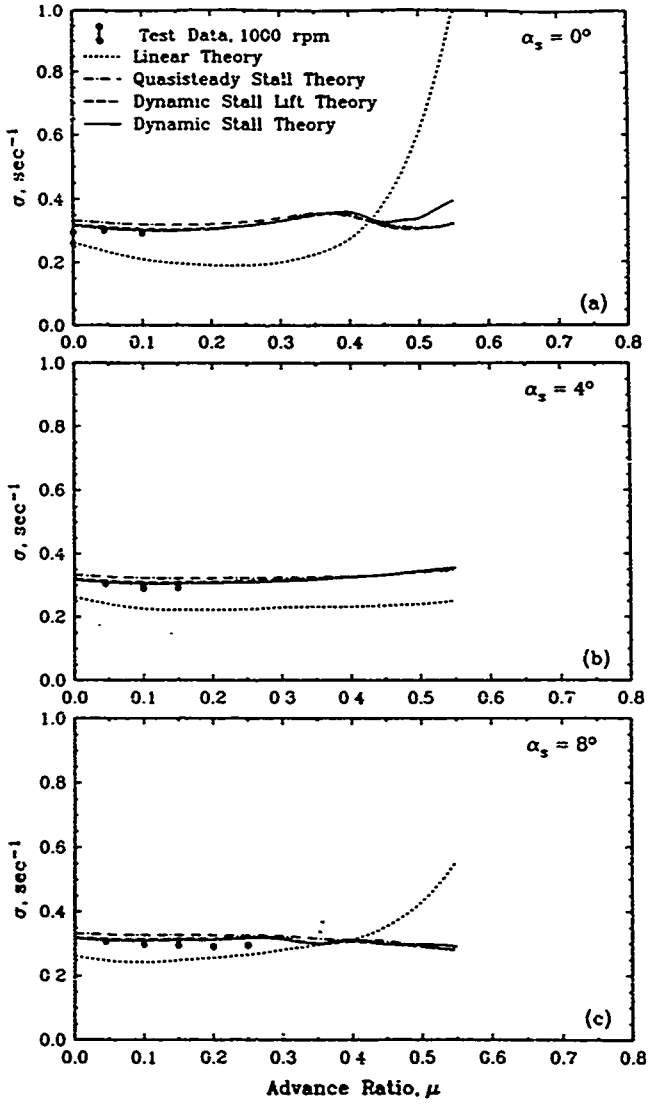

Fig. 12 : Lag Damping Correlation in Forward Flight for Low Shaft Angles, $\theta_o = 3°$

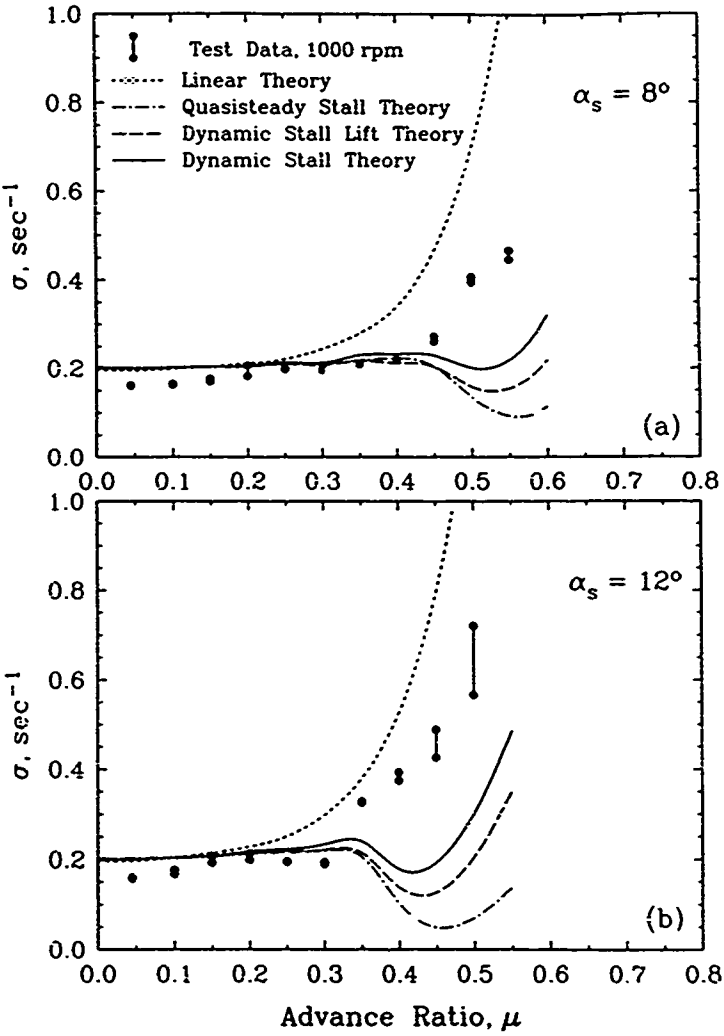
Test Data, 1000 rpm
Linear Theory
Quasisteady Stall Theory
Dynamic Stall Lift Theory
Dynamic Stall Theory
α_s = 8°
(a)
α_s = 12°
(b)
σ, sec⁻¹
Advance Ratio, μ
0.0
0.2
0.4
0.6
0.8
1.0
0.1
0.3
0.5
0.7

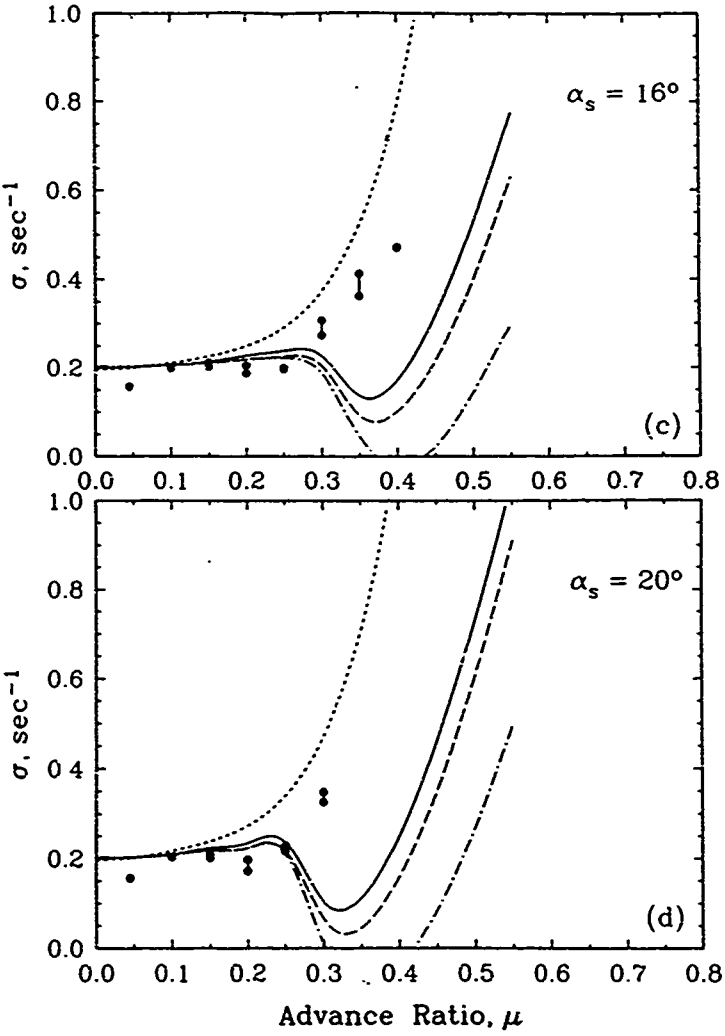

Fig 13. Lag Damping Correlation in Forward Flight for High Shaft Angles, $\theta_o = 0^c$

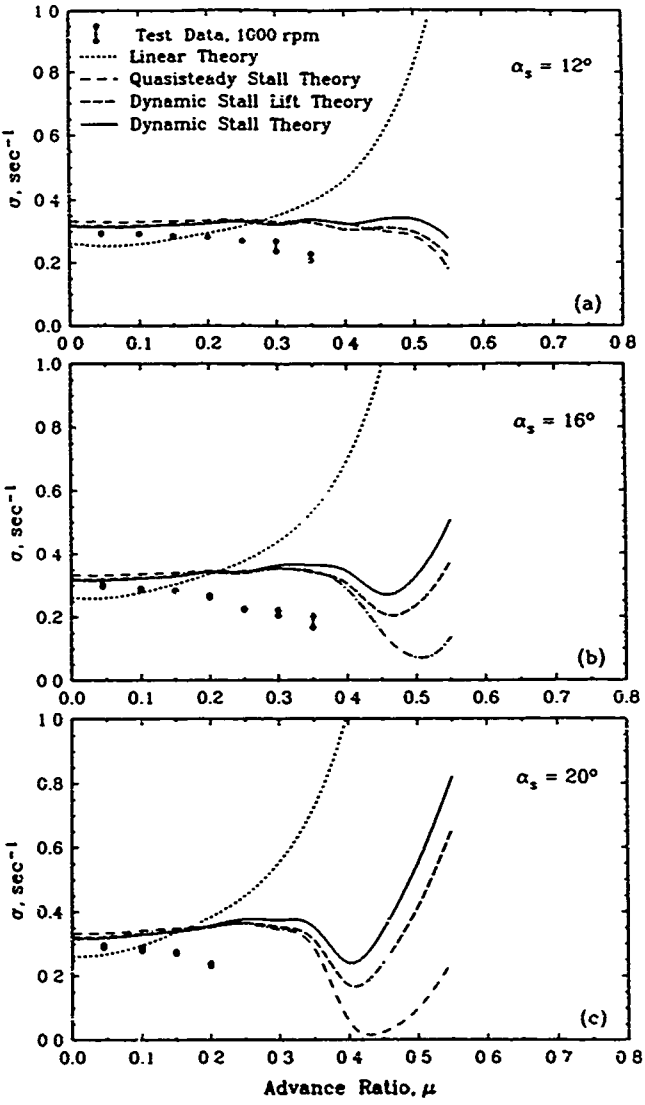

Fig. 14 · Lag Damping Correlation in Forward Flight for High Shaft Angles, $\theta_0 = 3°$

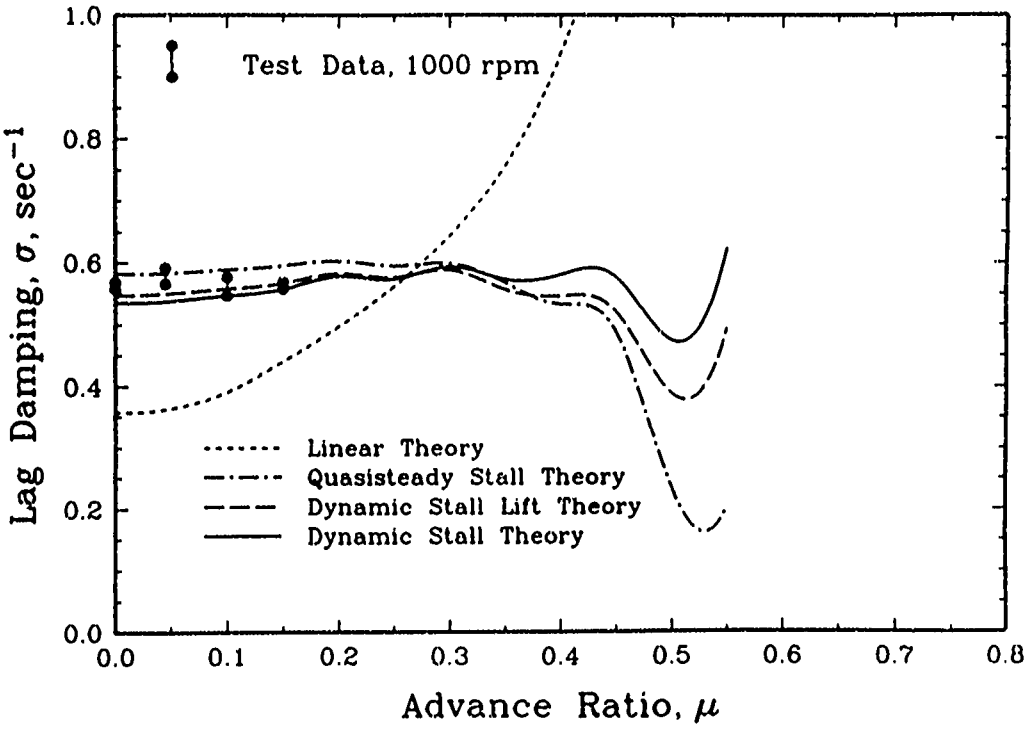

Fig. 15 : Lag Damping Correlation in Forward Flight, $\theta_o = 6°$, $\alpha_s = 20°$

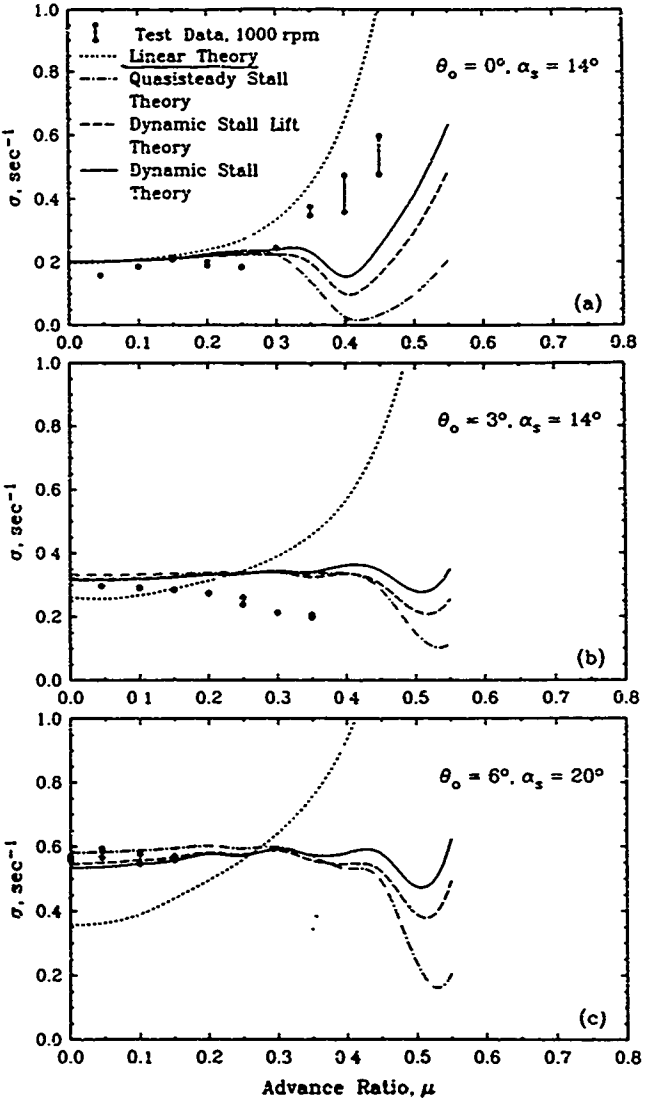

Fig 16 Summary of Lag Damping Correlation in Forward Flight

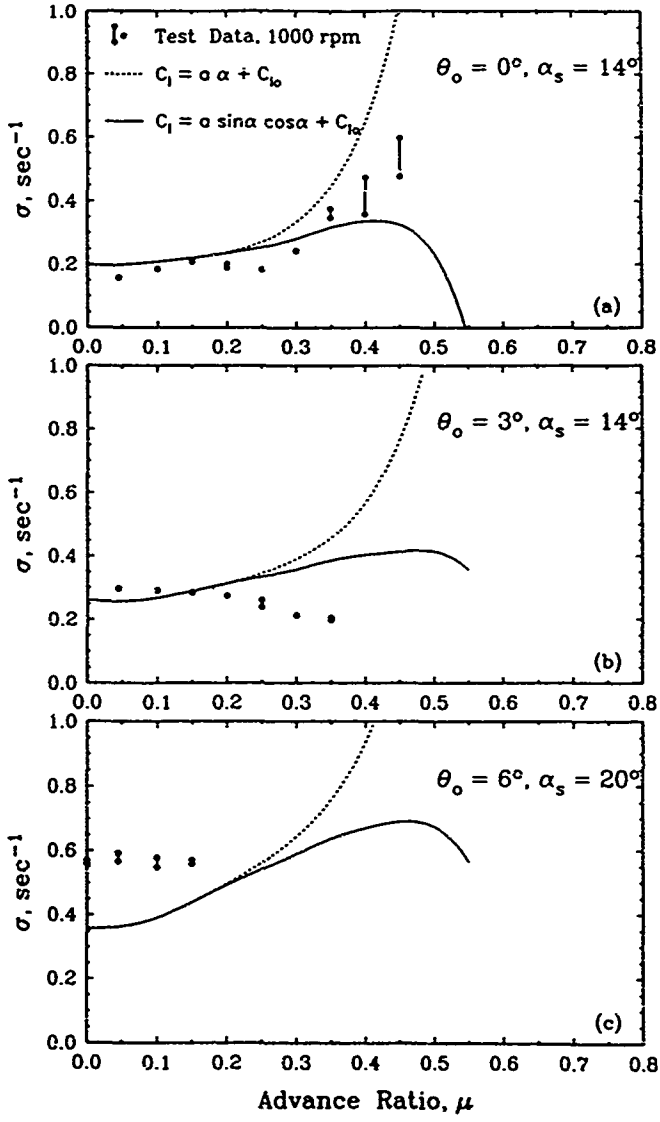

Fig. 17 : Adequacy of Linear Theory in Forward Flight

List of Publications

Following is the list of manuscripts submitted or published under ARO sponsorship during the period of this research work (including journal references):

1) "An Experimental an Analytical Investigation of Stall Effects on Flap-Lag Stability in Forward Flight", 13th European Rotorcraft Forum, Paper No. 6-2, 1987.
2) "An Experimental and Analytical Investigation of Isolated Rotor Flap-Lag Stability in Forward Flight", Journal of American Helicopter Society, Vol. 35, (2), May 1990.
3) "A Study of Symbolic Processing and Computational Aspects in Helicopter Dynamics", Journal of Sound and Vibration, Vol 137, (3), March 1990.
4) "Prediction of Inplane Damping from Deterministic and Stochastic Models", Vertica, Vol 13, (2), July 1990.
5) "An Experimental and Analytical Investigation of Dynamic Stall Effects on Isolated Rotor Flap-Lag Stability", 46th AHS National Forum, Washington, DC, May 1990
6) "Effects of Rotating Frame Turbulence and Dynamic Stall on Gust Response of Helicopter Blades", 15th European Rotorcraft Forum, Amsterdam, September 1990

List of Personnel Supported

The estimated level of effort for this contract is about 40 man-months including the efforts of the principal investigator, Prof. Gopal H. Gaonkar The students supported by this project are as follows:

- Mr. C. S. Nagaraj, from Summer 1987 (left the Ph.D. program in Spring 1989)*.
- Mr. Dinesh Barwey, Ph.D. student, since Fall 1987*.
- Mr. R. Madhavan, M.S. Degree completed in Spring 1990*
- Mr. N. S. Achar, Ph.D. student, since Fall 1990*.
- Mr. V. V. George, M.S. Degree completed in Dec. 1990, partial summer support in 1990*.

*partially supported by the Mechanical Engineering Department, Florida Atlantic University.